Chemical Science

EDGE ARTICLE

View Article Online
View Journal | View Issue

Cite this: *Chem. Sci.*, 2019, **10**, 5699

All publication charges for this article have been paid for by the Royal Society of Chemistry

Diketopyrrolopyrrole-based fluorescence probes for the imaging of lysosomal Zn^{2+} and identification of prostate cancer in human tissue†

Chenchen Du,‡[a] Shibo Fu,‡[b] Xiaohua Wang,[a] Adam C. Sedgwick,[c] Wei Zhen,[a] Minjie Li,[a] Xinqiang Li,[d] Juan Zhou,*[b] Zhong Wang,*[b] Hongyu Wang*[a] and Jonathan L. Sessler*[ac]

Received 7th March 2019
Accepted 1st May 2019

DOI: 10.1039/c9sc01153f

rsc.li/chemical-science

A series of diketopyrrolopyrrole-based fluorescent probes (**DPP-C2**, **LysoDPP-C2**, **LysoDPP-C3**, and **LysoDPP-C4**) have been developed for the detection of low pH and Zn^{2+} in an AND logic fashion. The chelation of Zn^{2+} or the protonation of a morpholine moiety within these probes results in a partial increase in the fluorescence intensity, an effect ascribed to suppression of one possible photo-induced electron transfer (PET) pathway. In contrast, a large increase in the observed fluorescence intensity is observed at low pH and in the presence of Zn^{2+}; this is rationalized in terms of both possible PET pathways within the probes being blocked. Job plots, fluorescence titration curves, and isothermal titration calorimetry proved consistent with a 1 : 1 Zn^{2+} complexation stoichiometry. Each probe demonstrated an excellent selectivity towards Zn^{2+} and the resulting Zn^{2+} complexes demonstrated pH sensitivity over the 3.5–9 pH range. Fluorescence imaging experiments confirmed that **LysoDPP-C4** was capable of imaging lysosomal Zn^{2+} in live cells. Little evidence of cytotoxicity was seen. **LysoDPP-C4** was successfully applied to the bioimaging of nude mice, wherein it was shown capable of imaging the prostate. Histological studies using a human sample revealed that **LysoDPP-C4** can discriminate cancerous prostate tissue from healthy prostate tissue.

Introduction

Zinc (Zn^{2+}) is one of the most common d-block metals found in the human body. It plays an important role in a wide range of biochemical processes and is used to maintain the structural integrity of over 3000 human proteins.[1] In addition, so-called labile Zn^{2+} ions are commonly found in specific areas of the human body, including the prostate.[2] In the prostate, Zn^{2+} is found at concentrations between ~10 to 100 mM.[3,4] This high Zn^{2+} concentration serves to inhibit *m*-aconitase activity thus preventing citrate oxidation during the Krebs cycle.[2,5,6] This unique function allows increased production and secretion of citrate into the prostatic fluid and is considered vital for the normal function of the prostate. However, in malignant prostate tissue, there is a dramatic decrease in Zn^{2+} concentration (500 nmol g^{-1} *vs.* 3000 nmol g^{-1} – for malignant and healthy tissues, respectively), as well as a downregulation of the zinc transporter, ZIP1.[7–10] Indeed, strong correlations between prostatic Zn^{2+} levels and prostate cancer (PCa) have been reported.[5] These correlations are providing an incentive to develop probes for Zn^{2+} that may be used to image the prostate and differentiate between normal and cancerous tissues in biopsy samples. Here, we report initial efforts to develop such a probe.

To date, considerable effort has been devoted to the development of Zn^{2+} probes.[11–20] Fluorescence-based systems have received particular attention in this regard since they provide good sensitivity, selectivity, and spatial and temporal resolution. In 2010, Lippard, *et al.* reported the fluorescence Zn^{2+} probe, ZPP1, which was successfully used to identify PCa in a transgenic mouse model.[21] Subsequently, they developed a triphenylphosphonium (TPP) functionalized, reaction-based fluorescent probe (DA-ZP1-TPP), which selectively localized at the mitochondria. On the basis of studies with this probe, it was concluded that tumorigenic cancer cells are unable to accumulate Zn^{2+} within their mitochondria.[22] More recently, Liu, *et al.* reported the Zn^{2+} sensor 3HC-DPA. This system relies on ESIPT (excited-state intramolecular proton transfer)[23] to distinguish between

[a]*Department of Chemistry, College of Science, Center for Supramolecular Chemistry & Catalysis, Shanghai University, 99 Shangda Road, Shanghai, 200444, P. R. China. E-mail: wanghy@shu.edu.cn*

[b]*Department of Urology, Shanghai Ninth People's Hospital, Shanghai Jiaotong University, School of Medicine, Shanghai, 200011, P. R. China*

[c]*Department of Chemistry, The University of Texas at Austin, 105 E 24th Street A5300, Austin, TX 78712-1224, USA. E-mail: sessler@cm.utexas.edu*

[d]*Pathology Department, First Affiliated Hospital of Zhengzhou University, 1 Jianshe East Road, Zhengzhou, Henan Province, 450052, P. R. China*

† Electronic supplementary information (ESI) available: Synthetic procedures, ^{1}H, ^{13}C NMR, and mass spectra, UV-Vis and fluorescence spectroscopic analyses, and other materials. See DOI: 10.1039/c9sc01153f

‡ Both authors contributed equally to this work.

cancerous prostate cells and healthy prostate cells.[24] To our knowledge no known Zn^{2+} sensor has been applied to the problem of prostate tissue differentiation in human samples. Moreover, systems capable of detecting zinc cation concentrations in an organelle-selective way are still limited.[22]

Lysosomes are acidic organelles with a pH (3.5–6.0) that is distinctly lower than that of the cytoplasm (pH 7.2). Within the acidic lysosomal environment, a diversity of functions is maintained, such as the digestion and degradation of macromolecules by hydrolytic enzymes. These lysosomal functions are closely linked to other cell processes, including plasma membrane repair and metabolism.[25] The abnormal function of lysosomes has been linked to the pathogenesis of a number of disorders and diseases.[25,26] Probes that provide insight into the functioning of lysosomes may thus have a role to play in the diagnostic and staging of various diseases, including cancer.

To our knowledge, there are currently no fluorescent probes that may be used to image lysosomal Zn^{2+} in prostate cancer cells. We believe that a dual detection strategy that monitors both pH and Zn^{2+} concentrations may allow this goal to be achieved. In recent years several research groups have focused on applying molecular logic to the problem of biological sensing.[27–30] So-called AND logic-based fluorescence probes are particularly attractive since they may allow two or more biological analytes to be analysed simultaneously. In this work, we focused on the development of lysosomal targeting AND logic-based fluorescence probes for the detection of both acidic pH and Zn^{2+} (probes **DPP-C2**, **LysoDPP-C2**, **LysoDPP-C3**, and **LysoDPP-C4**; Fig. 1). This AND logic approach is designed to overcome the limitations associated with monitoring Zn^{2+} concentrations in the lysosome by increasing the signal-to-noise ratio between the lysosome (low pH – strong fluorescence) and cytosol (weak fluorescence).[31–33]

Results and discussion

To obtain probes with dual Zn^{2+} and H^+ sensing functions, both a methoxy-based *N*,*N*-di-(2-picolyl)ethylenediamine (MeO-DPEN) Zn^{2+} chelator[34] and a lysosome-targeting morpholine moiety were appended synthetically to the lactam units of a 3,6-diphenyl diketopyrrolopyrrole (DPP) fluorophore (Fig. 1). Each of these functionalities was designed to quench the fluorescence *via* an independent photoinduced electron transfer (PET) pathway. In the presence of Zn^{2+}, MeO-DPEN forms a chelate complex with the Zn^{2+} cation. This results in a partial increase in the fluorescence emission intensity through inhibition of the PET process associated with this particular subunit. When the resulting Zn^{2+} probe complex is exposed to an acidic environment (*e.g.*, enters the lysosome), the morpholine unit becomes protonated; this leads to a complete restoration of the fluorescence emission intensity since both PET pathways are now blocked. The basic mechanistic rationale underlying our probe design and expected function is shown in Scheme 1.

The synthesis of probes **DPP-C2**, **LysoDPP-C2**, **LysoDPP-C3**, and **LysoDPP-C4** is detailed in the ESI (Schemes S1–S3†). In brief, dye **1** was asymmetrically acylated under basic conditions with *tert*-butyl bromoacetate to afford intermediate **2** in 25% yield. Compound **2** was then alkylated with bromoethane or bromo-substituted alkyl morpholine intermediates containing tethers of varying lengths ($n = 2$ and 3; precursors **3** and **4**) using K_2CO_3 as a base, NaI as a catalyst, and acetone as the solvent to afford compounds **5**, **6** and **7** in 56–60% yield. To access the alkyl ($n = 4$) morpholine functionalized DPP, intermediate **2** was alkylated with 1,4-dibromobutane using similar alkylation conditions. This afforded the bromo-alkyl intermediate **8**, which was subsequently reacted with morpholine, giving compound **9** in excellent yield (79%). The *tert*-butyl esters of intermediates **5**, **6**, **7**, and **9** were hydrolysed using trifluoroacetic acid to give the corresponding free carboxylic acids. Each

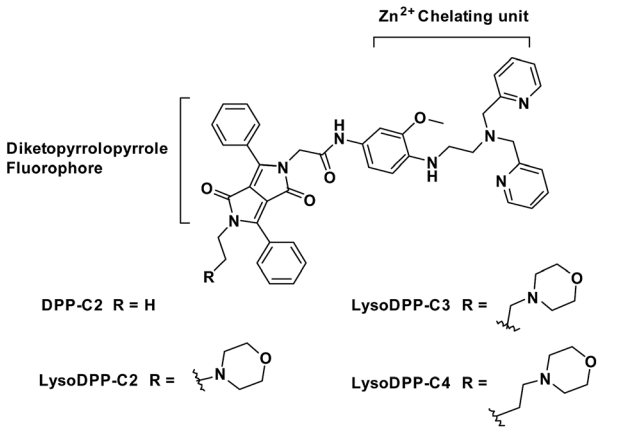

Fig. 1 The development of dual-functionalized diketopyrrolopyrrole (DPP)-based fluorescent probes for the AND logic-based detection of both acidic pH and Zn^{2+}.

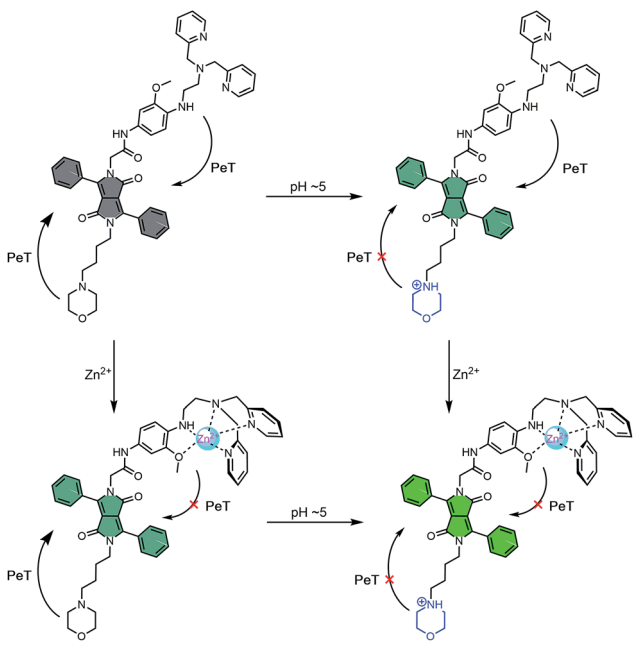

Scheme 1 Fluorescence 'turn on' mechanism allowing for the concurrent detection of low pH AND Zn^{2+}. Grey – weak fluorescence emission intensity. Green – strong fluorescence emission intensity.

carboxylic acid was taken onto the next step without purification and reacted with amino functionalized MeO-DPEN to yield the desired AND logic fluorescent probes **DPP-C2**, **LysoDPP-C2**, **LysoDPP-C3**, and **LysoDPP-C4**.

With each probe in hand, UV-Vis and fluorescence spectroscopic analyses were performed. The polarity of the solvent was shown to have little effect on the UV-Vis absorption or fluorescence emission spectrum of each probe or the corresponding Zn^{2+}/probe complex (Fig. S1–S4, Tables S1 and S2†). Interestingly, the **DPP-C2**/Zn^{2+} complex demonstrated poor photostability with the intensity of the UV-Vis absorption and fluorescence maxima being reduced by 58% and 41%, respectively, after one week of exposure to sun light. In contrast, the morpholine-functionalized probes exhibited greater photostability with only a 33%, 26% and 20% reduction in fluorescence emission maxima being seen for **LysoDPP-C2**/Zn^{2+}, **LysoDPP-C3**/Zn^{2+}, and **LysoDPP-C4**/Zn^{2+}, respectively, after a similar week of exposure to sun light (Fig. S5 and S6†).

The Zn^{2+} affinity of each probe was then assessed. As prepared, each probe proved relatively non-fluorescent (Φ_F below 0.8%). However, treatment with Zn^{2+} ($ZnSO_4$) resulted in an increase in fluorescence intensity. Through quantitative fluorescence titrations with corresponding good fits to a 1 : 1 binding profile, it was determined that all four probes responded to nanomolar concentrations of Zn^{2+} (K_d = 2.83, 1.54, 2.57, and 1.91 nm for **DPP-C2**, **LysoDPP-C2**, **LysoDPP-C3**, and **LysoDPP-C4**, respectively; see Fig. S7–S13†). Job plot analyses provided support for the proposed 1 : 1 stoichiometry. The ability to interact with Zn^{2+} was further confirmed through isothermal titration calorimetry (ITC) (Fig. S14 and S15†).

Next, we evaluated the ability of each probe to detect Zn^{2+} at different pH. As shown in Fig. 2, S16 and S17,† the probes proved non-fluorescent in aqueous solution over the 6.5–9 pH range. As expected, the addition of Zn^{2+} (1 μM) to the non-morpholine functionalized control **DPP-C2** probe resulted in the complete restoration of the fluorescence emission intensity. This system also proved insensitive to pH (3.5–9). In contrast, the addition of Zn^{2+} (1 μM) to the morpholine-functionalized probes (**LysoDPP-C2** and **LysoDPP-C4**) over a pH range of 6.5–9 led to an increase in the fluorescence intensity with the largest fluorescence response being produced by **LysoDPP-C4**. As the pH gradually became more acidic, the Zn^{2+} complex of **LysoDPP-C2** produced the greatest change in fluorescence intensity. Moreover, the extent of PET fluorescence quenching was found to decrease as the distance between the DPP subunit and the morpholine moiety increased. Per the design expectations, each morpholine-functionalized probe displayed a low fluorescence emission intensity at cytosolic pH and strong fluorescence emission intensity at lysosomal pH and in the presence of Zn^{2+}. These results were considered as important predicates to achieving lysosomal Zn^{2+} imaging with a good signal to noise ratio.

Prior to cellular studies of each probe, metal cation selectivity and competition experiments were performed. As shown in Fig. S18,† no competition involving Zn^{2+} binding was observed for the commonly found biological metal ions Na^+, Ca^{2+}, K^+, and Mg^{2+} in the case of any of the probes. However, the metal ions Mn^{2+}, Fe^{2+}, Fe^{3+}, Co^{2+}, Ni^{2+}, Cu^{2+}, and Cd^{2+} resulted in partial or total fluorescence quenching. Due to the absolute or labile (free) concentrations of these cations being relatively low in cells, we do not believe they would provide a source of interference in the context of lysosomal Zn^{2+} analyses.

Each probe was then evaluated *in vitro*. Here, HeLa cells were used as a model system to evaluate cytotoxicity, responsiveness to intracellular Zn^{2+}, and lysosomal targeting. Low cytotoxicity was observed for each probe (Fig. S19†). They were thus used for cellular imaging experiments. As illustrated in Fig. 3, upon incubation the fluorescence produced by both **DPP-C2** and **LysoDPP-C4** was appreciable, whereas **LysoDPP-C2** and **LysoDPP-C3** were characterized by low levels of fluorescence emission intensity. Upon the addition of *N*,*N*,*N*′,*N*′-tetrakis(2-pyridylmethyl) ethylenediamine (TPEN), a membrane permeable zinc chelator,[35] a decrease in the fluorescence emission intensity was observed in the case of each probe. In contrast, the addition of Zn^{2+} in the form of zinc/pyrithione (ZnPT)[36] led to a remarkable increase in the fluorescence intensity. On this basis, we concluded

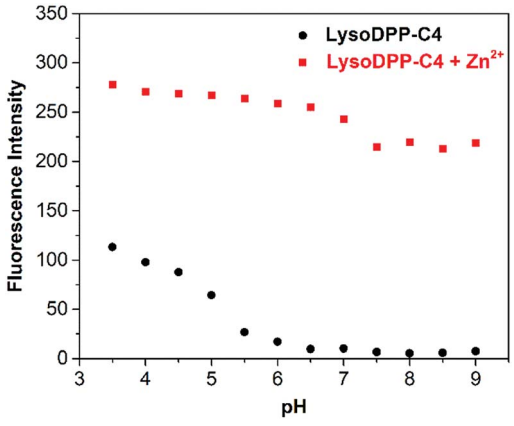

Fig. 2 Fluorescence intensity of **LysoDPP-C4** (1 μM) and its zinc complex in solutions of varying pH (0.05 M NaCl aqueous solution). λ_{ex} = 430 nm/λ_{em} = 515 nm.

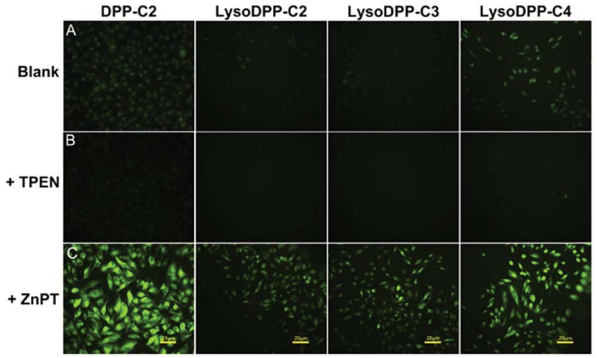

Fig. 3 Fluorescent microscope images of HeLa cells. (Row A) Cells incubated with 10 μM of the indicated probe for 24 h; (Row B) cells incubated with 10 μM of the indicated probe for 24 h, followed by further incubation with 50 μM TPEN for 10 min; (Row C) cells incubated with 10 μM of the indicated probe for 24 h, followed by further incubation with a mixture of 60 μM ZnPT for 10 min.

that probe **LysoDPP-C4**, in particular, was worth pursuing further as a dual mode (AND logic) intracellular Zn^{2+} sensor. On the other hand, probes **LysoDPP-C2** and **LysoDPP-C3** were not pursued further due to their inability to produce a presumed zinc cation-based background fluorescence response.

The subcellular distributions of **LysoDPP-C4** and the control probe **DPP-C2** were then determined through co-staining experiments with LysoTracker™ Red DND-99 (Fig. 4). **LysoDPP-C4** was shown to localize at the lysosome through a close overlap with LysoTracker™ Red DND-99 producing a Pearson's coefficient (*A*) of 0.68 (Fig. 4d). In accord with the design expectation that the morpholine functionality present in **LysoDPP-C4** was largely responsible for the observed lysosomal targeting, the morpholine-free control **DPP-C2** was shown to have a poor overlap with LysoTracker™ Red DND-99 (Pearson's coefficient of 0.17; Fig. 4h).

LysoDPP-C4 was then tested for its ability to discriminate between cancerous and normal prostate cells. Toward this end, two prostate cancerous cell lines PC3 and DU145 and one normal human prostate epithelial cell line, RWPE1, were used. **LysoDPP-C4** showed negligible cytotoxicity towards these prostate cell lines (Fig. S20†). Addition of Zn^{2+} to the cancerous cells DU145 and PC3 resulted in no change in the fluorescence intensities. However, the addition of Zn^{2+} to RWPE1 cells resulted in a significant increase in the observed fluorescence intensity (Fig. 5). This difference is ascribed to the down-regulation of zinc transporters in cancerous PC3 and DU145 cells, which reduces the uptake of extracellular Zn^{2+}.

Support for these findings came from flow cytometry and ICP-MS analyses. These studies revealed that the zinc concentration-dependent fluorescence enhancement could be observed only in RWPE1 cells after incubation with Zn^{2+} (15 μM), which afforded a 5.9-fold fluorescence increase. An approximate 2.5-fold increase in $[Zn^{2+}]$ in RWPE1 cells was estimated by ICP-MS using Sr^{2+} as the internal standard (Fig. S21 and Table S3†). On this basis, we conclude that **LysoDPP-C4** may be used to discriminate between healthy and cancerous prostate cells.

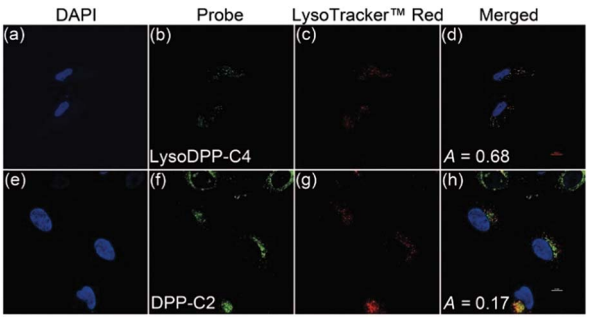

Fig. 4 Co-localization images of HeLa cells incubated with **DPP-C2** or **LysoDPP-C4** (10 μM, 24 h) and LysoTracker™ Red DND-99 (50 nM, 2.5 h). (a and e) The nuclei of the cells (blue) were stained by the blue fluorescent dye, 4,6-diamidino-2-phenylindole (DAPI). (b and f) Stained by **LysoDPP-C4** and **DPP-C2**, respectively. (c and g) Stained by LysoTracker™ Red DND-99. (d) Merged image of (b) and (c). (h) Merged image of (f) and (g).

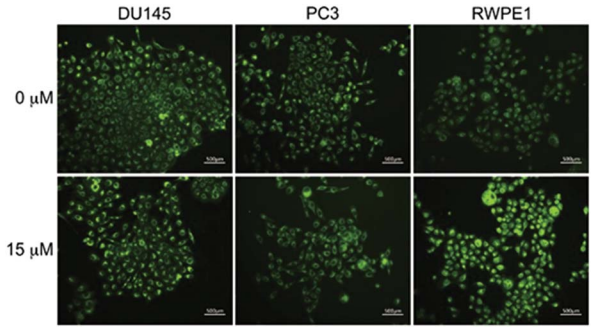

Fig. 5 Fluorescence microscope images of cancerous prostate cells, PC3 and DU145, and normal human prostate epithelial cells, RWPE1, incubated with **LysoDPP-C4** (1 μM, 24 h) in the absence and presence of an exogenous zinc source (15 μM – $ZnSO_4$).

On the basis of these *in vitro* studies, **LysoDPP-C4** was tested *in vivo* using nude mice models (Fig. 6). As can be seen from an inspection of Fig. 6b, injection of **LysoDPP-C4** (500 μg per mouse, 5 mice per set) into male BALB/c nude mice *via* the tail vein resulted in a bright fluorescence signal in the region of the prostate after 15 minutes. The mice were then sacrificed and dissected. The viscera were observed using a fluoroscope. Both white-light color images and fluorescent images were taken under the same settings (Fig. 6c and d). The prostate and seminal vesicle displayed a strong green fluorescence, which is consistent with both literature reports that a high concentration of Zn^{2+} are found in these organs and the central hypothesis underlying the present study, namely that **LysoDPP-C4** is functioning as an effective Zn^{2+} probe.

Histological analyses were then carried out and served to confirm the above observations (Fig. 6e). For instance, frozen sections of the prostate and seminal vesicle produced a strong green fluorescence signal, whereas little fluorescence was observed in the case of the liver and kidney sections. Essentially

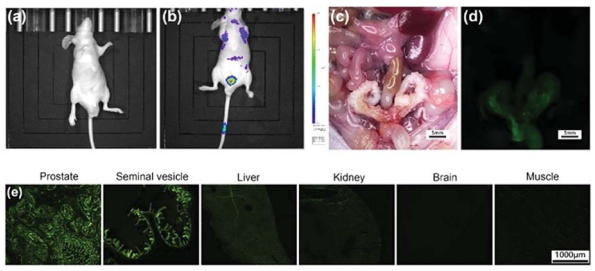

Fig. 6 Representative *in vivo* whole-body epi-fluorescence optical imaging of tumor-free male BALB/c nude mice before injection (a) and 15 minutes after tail-vein injection (b) of **LysoDPP-C4** (500 μg per mouse). There was a strong fluorescence signal enhancement in the prostate-associated area after injection. The treated mouse was sacrificed and dissected. The excised prostate and seminal vesicles revealed bright green fluorescence upon irradiation at the tetraethyl rhodamine isothiocyanate (TRITC) excitation wavelength, while other viscera and skeletal muscle remained dark (c and d). *Ex vivo* fluorescence optical imaging of the prostate, seminal vesicles, liver, kidney, brain and adjacent muscle tissue obtained from the mouse injected with **LysoDPP-C4** (e).

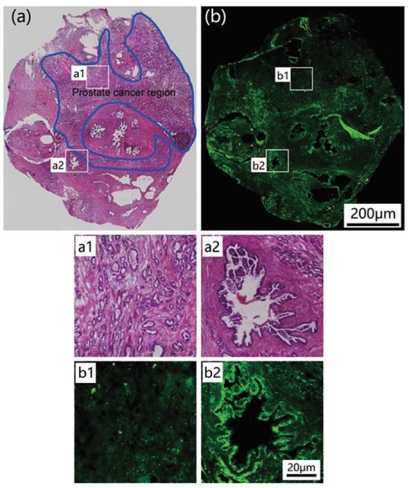

Fig. 7 Histological analysis. (a) Image of a prostate nodule sections stained by H & E staining. The cancerous region is indicated by the blue line. (b) Fluorescence staining of the same nodule using **LysoDPP-C4**. Regions of interest (a1) and (b1) reflect cross-sectional cancerous prostate nodules stained by H & E staining and **LysoDPP-C4**, respectively. Regions of interest (a2) and (b2) are cross-sectional views of normal prostate nodules stained by H & E staining and **LysoDPP-C4**, respectively.

no fluorescence emission was observed in the case of the brain and muscle samples. These results provide support for our contention that **LysoDPP-C4** may be used to image the prostate *via* Zn^{2+}-induced fluorescence signaling.

To test the potential of **LysoDPP-C4** in prostate cancer biomedical imaging applications, a prostate nodule obtained from a 65 year-old male patient diagnosed with prostate cancer (Gleason's score, 3 + 3) was used. First, hematoxylin and eosin (H & E) staining was used to highlight the cancerous region (area within the blue line in Fig. 7a). Subsequent staining with **LysoDPP-C4** allowed a clear visualization of the cancerous regions as shown by regions of relatively low fluorescence emission intensity (Fig. 7b). A significant difference in fluorescence intensity between healthy and cancerous tissue was observed. Therefore, we propose that **LysoDPP-C4** may have a role to play in identifying cancerous prostate tissue in human samples.

Experimental

All animal experiments were performed according to the Chinese Regulations for the Administration of Affairs Concerning Experimental Animals and approved by the Subcommittee on Research Animal Care at the Shanghai Ninth People's Hospital. All experimental details are provided in the ESI.†

All animal experiments were performed in accord with institutional guidelines and were specifically approved by the Subcommittee on Research Animal Care at the Shanghai Ninth People's Hospital.

Conclusions

In summary, we report here a series of diketopyrrolopyrrole-based AND logic fluorescent probes (**DPP-C2**, **LysoDPP-C2**, **LysoDPP-C3** and **LysoDPP-C4**) that were designed to permit the detection of both low pH and Zn^{2+} in an AND logic-like fashion. In these probes, the aliphatic morpholine moiety serves as both a pH-responsive marker and a lysosome-targeting subunit. Chelation of Zn^{2+} or the protonation of the morpholine moiety serves to suppress only one PET pathway, resulting in a small increase in the observed fluorescence intensity. However, when both PET pathways are blocked, as occurs in the presence of Zn^{2+} and H^+, the fluorescence is fully recovered. The effectiveness of this strategy in terms of sensing was demonstrated through lysosomal Zn^{2+} imaging in live cells. The most effective probe in terms of both initial fluorescence intensity and Zn^{2+}-induced increases proved to be **LysoDPP-C4**. This system demonstrated low cytotoxicity and permitted changes in intracellular Zn^{2+} concentrations in the lysosome to be monitored. **LysoDPP-C4** could be used to discriminate between cancerous and normal prostate cells. *In vivo* and histological studies demonstrated the effectiveness of **LysoDPP-C4** in terms of identifying the prostate and to delineating cancerous regions within a prostate cancer sample obtained from a 65 year old male patient.

Conflicts of interest

There are no conflicts to declare.

Acknowledgements

This work was financially supported by the National Natural Science Foundation of China (61774099, 81402089) and Program for Outstanding Medical Academic Leader. The work in Austin was supported by the National Institutes of Health (CA68682 to JLS) and the Robert A. Welch Foundation (F-0018 to JLS).

Notes and references

1 A. Krezel and W. Maret, *Arch. Biochem. Biophys.*, 2016, **611**, 3–19.
2 L. C. Costello and R. B. Franklin, *Prostate*, 1998, **35**, 285–296.
3 F. Gyorkey, K. W. Min, J. A. Huff and P. Gyorkey, *Cancer Res.*, 1967, **27**, 1348–1353.
4 M. V. C. Jordan, S. T. Lo, S. W. Chen, C. Preihs, S. Chirayil, S. R. Zhang, P. Kapur, W. H. Li, L. M. De Leon-Rodriguez, A. J. M. Lubag, N. M. Rofsky and A. D. Sherry, *Proc. Natl. Acad. Sci. U. S. A.*, 2016, **113**, E5464–E5471.
5 L. C. Costello, P. Feng, B. Milon, M. Tan and R. B. Franklin, *Prostate Cancer Prostatic Dis.*, 2004, **7**, 111–117.
6 L. C. Costello and R. B. Franklin, *Arch. Biochem. Biophys.*, 2016, **611**, 100–112.
7 R. B. Franklin, P. Feng, B. Milon, M. M. Desouki, K. K. Singh, A. Kajdacsy-Balla, O. Bagasra and L. C. Costello, *Mol. Cancer*, 2005, **4**, 32.
8 L. C. Costello and R. B. Franklin, *J. Biol. Inorg Chem.*, 2011, **16**, 3–8.
9 V. Kolenko, E. Teper, A. Kutikov and R. Uzzo, *Nat. Rev. Neurol.*, 2013, **10**, 219–226.

10 L. C. Costello, R. B. Franklin and P. Feng, *Mitochondrion*, 2005, **5**, 143–153.
11 D. Wu, A. C. Sedgwick, T. Gunnlaugsson, E. U. Akkaya, J. Yoon and T. D. James, *Chem. Soc. Rev.*, 2017, **46**, 7105–7123.
12 J. M. Goldberg, F. Wang, C. D. Sessler, N. W. Vogler, D. Y. Zhang, W. H. Loucks, T. Tzounopoulos and S. J. Lippard, *J. Am. Chem. Soc.*, 2018, **140**, 2020–2023.
13 M. L. Zastrow, R. J. Radford, W. Chyan, C. T. Anderson, D. Y. Zhang, A. Loas, T. Tzounopoulos and S. J. Lippard, *ACS Sens.*, 2016, **1**, 32–39.
14 K. P. Carter, M. C. Carpenter, B. Fiedler, R. Jimenez and A. E. Palmer, *Anal. Chem.*, 2017, **89**, 9601–9608.
15 Y. Han, J. M. Goldberg, S. J. Lippard and A. E. Palmer, *Sci. Rep.*, 2018, **8**, 15034.
16 K. A. Jolliffe, *Acc. Chem. Res.*, 2017, **50**, 2254–2263.
17 L. Fang, G. Trigiante, C. J. Kousseff, R. Crespo-Otero, M. P. Philpott and M. Watkinson, *Chem. Commun.*, 2018, **54**, 9619–9622.
18 W. Jiang, Q. Q. Fu, H. Y. Fan and W. Wang, *Chem. Commun.*, 2008, 259–261.
19 H. A. Michaels, C. S. Murphy, R. J. Clark, M. W. Davidson and L. Zhu, *Inorg. Chem.*, 2010, **49**, 4278–4287.
20 L. Zhu, Z. Yuan, J. T. Simmons and K. Sreenath, *RSC Adv.*, 2014, **4**, 20398–20440.
21 S. K. Ghosh, P. Kim, X. A. Zhang, S. H. Yun, A. Moore, S. J. Lippard and Z. Medarova, *Cancer Res.*, 2010, **70**, 6119–6127.
22 W. Chyan, D. Y. Zhang, S. J. Lippard and R. J. Radford, *Proc. Natl. Acad. Sci. U. S. A.*, 2014, **111**, 143–148.
23 A. C. Sedgwick, L. L. Wu, H. H. Han, S. D. Bull, X. P. He, T. D. James, J. L. Sessler, B. Z. Tang, H. Tian and J. Yoon, *Chem. Soc. Rev.*, 2018, **47**, 8842–8880.
24 X. Li, J. Li, X. W. Dong, X. Gao, D. Zhang and C. L. Liu, *Sens. Actuators, B*, 2017, **245**, 129–136.
25 J. P. Luzio, P. R. Pryor and N. Bright, *Nat. Rev. Mol. Cell Biol.*, 2007, **8**, 622–632.
26 F. M. Platt, B. Boland and A. C. van der Spoel, *J. Cell Biol.*, 2012, **199**, 723–734.
27 S. Erbas-Cakmak, S. Kolemen, A. C. Sedgwick, T. Gunnlaugsson, T. D. James, J. Yoon and E. U. Akkaya, *Chem. Soc. Rev.*, 2018, **47**, 2228–2248.
28 J. L. Kolanowski, F. Liu and E. J. New, *Chem. Soc. Rev.*, 2018, **47**, 195–208.
29 A. Romieu, *Org. Biomol. Chem.*, 2015, **13**, 1294–1306.
30 H. M. Kim, M. S. Seo, M. J. An, J. H. Hong, Y. S. Tian, J. H. Choi, O. Kwon, K. J. Lee and B. R. Cho, *Angew. Chem., Int. Ed.*, 2008, **47**, 5167–5170.
31 H. Zhu, J. L. Fan, S. L. Zhang, J. F. Cao, K. D. Song, D. Ge, H. J. Dong, J. Y. Wang and X. J. Peng, *Biomater. Sci.*, 2014, **2**, 89–97.
32 C. C. Du, S. B. Fu, X. L. Ren, X. H. Wang, Z. Wang, J. Zhou and H. Y. Wang, *New J. Chem.*, 2018, **42**, 3493–3502.
33 H. J. Lee, C. W. Cho, H. Seo, S. Singha, Y. W. Jun, K. H. Lee, Y. Jung, K. T. Kim, S. Park, S. C. Bae and K. H. Ahn, *Chem. Commun.*, 2016, **52**, 124–127.
34 Z. C. Xu, J. Yoon and D. R. Spring, *Chem. Soc. Rev.*, 2010, **39**, 1996–2006.
35 S. L. Sensi, D. Ton-That, P. G. Sullivan, E. A. Jonas, K. R. Gee, L. K. Kaczmarek and J. H. Weiss, *Proc. Natl. Acad. Sci. U. S. A.*, 2003, **100**, 6157–6162.
36 B. L. Barnett, H. C. Kretschmar and F. A. Hartman, *Inorg. Chem.*, 1977, **16**, 1834–1838.